HHS Public Access

Author manuscript

ACS Nano. Author manuscript; available in PMC 2017 August 23.

Published in final edited form as:

ACS Nano. 2016 August 23; 10(8): 7721–7730. doi:10.1021/acsnano.6b03074.

Dual-Modality Positron Emission Tomography/Optical Image-Guided Photodynamic Cancer Therapy with Chlorin e6-Containing Nanomicelles

Liang Cheng[1,2], **Anyanee Kamkaew**[2], **Haiyan Sun**[2], **Dawei Jiang**[2], **Hector F. Valdovinos**[3], **Hua Gong**[1], **Christopher G. England**[3], **Shreya Goel**[4], **Todd E. Barnhart**[3], and **Weibo Cai**[2,3,4]

Liang Cheng: lcheng2@suda.edu.cn; Weibo Cai: wcai@uwhealth.org

[1]Institute of Functional Nano & Soft Materials (FUNSOM), Collaborative Innovation Center of Suzhou Nano Science and Technology, Soochow University, Suzhou, Jiangsu 215123, China

[2]Department of Radiology, University of Wisconsin-Madison, Wisconsin 53705, United States

[3]Department of Medical Physics, University of Wisconsin-Madison, Wisconsin 53705, United States

[4]Materials Science Program, University of Wisconsin–Madison, Wisconsin 53705, United States

Abstract

Multifunctional nanoparticles with combined diagnostic and therapeutic functions show great promise in nanomedicine. Herein, we develop an organic photodynamic therapy (PDT) system based on polyethylene glycol (PEG)-coated nanomicelles conjugated with ~20% of chlorin e6 (PEG-Ce 6 nanomicelles), which functions as an optical imaging agent, as well as a PDT agent. The formed PEG-Ce 6 nanomicelles with the size of ~20 nm were highly stable in various physiological solutions for a long time. Moreover, Ce 6 can also be a ^{64}Cu chelating agent for *in vivo* positron emission tomography (PET). By simply mixing, more than 90% of ^{64}Cu was chelator-free labeled on PEG-Ce 6 nanomicelles, and they also showed high stability in serum condition. Both fluorescence imaging and PET imaging revealed that PEG-Ce 6 nanomicelles displayed high tumor uptake (13.7 ± 2.2%ID/g) after intravenous injection into tumor-bearing mice at 48 h time point. In addition, PEG-Ce 6 nanomicelles exhibited excellent PDT properties upon laser irradiation, confirming the theranostic properties of PEG-Ce 6 nanomicelles for imaging and treatment of cancer. In addition, PDT was not shown to render any appreciable toxicity. This work presents a theranostic platform based on polymer nanomicelles with great potential in multimodality imaging-guided photodynamic cancer therapy.

Graphical Abstract

Correspondence to: Liang Cheng, lcheng2@suda.edu.cn; Weibo Cai, wcai@uwhealth.org.

Supporting Information

Supporting Information Available: Figures S1~S9 and Table S1. This material is available free of charge *via* the Internet at http://pubs.acs.org.

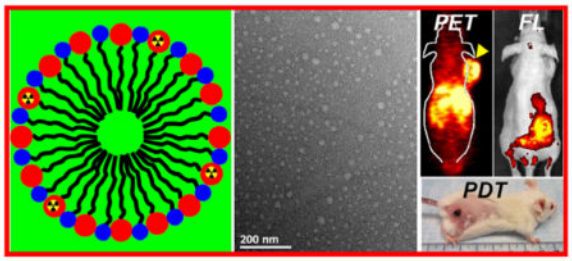

PEG-Ce 6 nanomicelles synthesized by simple conjugation polyethylene glycol with Ce 6 can be served as a ^{64}Cu chelating agent for *in vivo* PET/optical dual-modality image and photodynamic cancer therapy. Our work presents a theranostic platform based on polymer nanomicelles with great potential in multi-modality image-guided cancer therapy.

Keywords

PEG-Ce 6 nanomicelles; PET imaging; fluorescence imaging; EPR effect; photodynamic therapy

As of 2012, cancer has overtaken heart disease to become the leading cause of death worldwide, claiming the lives of nearly 8.2 million people each year.[1] While therapeutic strategies have undergone significant improvements over the last decade, cancer rates are expected to increase by 50% to 15 million new cases in the year 2020 according to the World Cancer Report.[2] Current clinical cancer therapies are limited to surgery, radiotherapy, and chemotherapy. Unfortunately, these approaches suffer from the risks of killing normal cells, destroying the immune system, and the formation of secondary cancers.[3, 4] Due to the invasive and ineffective approaches for cancer treatment, photodynamic therapy (PDT) is emerging as a powerful technique for cancer treatment.[5–7] In PDT, tumor cells are effectively eliminated by the generation of reactive oxygen species from the transfer of photo energy by the photosensitizer to surrounding oxygen molecules.[5, 8] Owing to the tumor targeting ability of appropriately designed photosensitizers agents and effective light irradiation methods, PDT exhibits high selective for malignant tissues and a remarkably reduced side effect profile in comparison to traditional methods.[9–11]

Moreover, image-guided therapy has been developed as a new concept in cancer treatment and shows promise in the optimization of therapeutic efficiency.[12–15] It can provide useful information regarding the size and location of tumors, the optimal time window for photo-therapy, and the monitoring of therapeutic efficacy. A variety of inorganic and organic-based photodynamic agents, such as gold nanostructures,[16–18] carbon-based nanomaterials,[19–21] mesoporous silica nanoparticles,[22, 23] upconversion nanoparticles,[24, 25] and polymer micelles[6, 26–30] have been widely explored by many research groups including ours for image-guided PDT. Although many of the above-mentioned materials have already shown high efficacies for image-guided photodynamic cancer therapy in pre-clinical animal experiments, most of these studies used inorganic photodynamic agents that are non-biodegradable and are retained in the body for long periods of time.[31, 32] Organic nanostructures have been utilized in cancer therapy due to their excellent biocompatibility and drug-loading capacity, however, most of them lack of imaging functions.[33–35] A few

organic photosensitizer nanoparticles, such as porphysome nanovesicles,[36, 37] polymer-Ce 6&IR825 nanocomplex,[38] and Abraxance-Ce 6 nanomicelles[39] have recently been proposed as theranostic agents for PDT or combined cancer therapy. Most of these nanostructures display high accumulation in liver and spleen despite active targeting, which is attributed in part to their relatively large size (~100 nm) that results in the nonspecific clearance by the reticuloendothelial system (RES).[38–40] Thus, it is of great importance to design an ideal nanoplatform displaying a smaller size and enhanced surface coating to avoid the RES. In addition, the nanoplatform must display excellent biocompatibility to prevent an immune response after injection and ensure potential clinical translation.

Nuclear imaging techniques such as positron emission tomography (PET) offer high spatial resolution and sensitivity as compared to other imaging modalities. PET imaging has been extensively employed in the field of molecular imaging for disease diagnosis, patient stratification, and monitoring of therapeutic efficacy.[41] Herein, we designed a type of polymer-Ce 6 nanomicelles for PET imaging, together with fluorescence (FL) image guided PDT. By simple conjugation of Ce 6 molecules to an amphiphilic polymer (C_{18}PMH-PEG-NH_2), PEG-Ce 6 nanomicelles were successfully synthesized with uniform size of ~20 nm. Without showing any appreciable toxicity to cells, PEG-Ce 6 nanomicelles could serve as an effective photodynamic agent to destruct cancer cells under NIR light. As the porphyrin structure of Ce 6, the synthesized PEG-Ce 6 nanomicelles acted as good chelating agent to label $^{64}Cu^{2+}$, a useful PET radionuclide with a 12.7 h half-life,[42] for PET imaging. By simple mixing, ^{64}Cu was successfully attached on the surface of PEG-Ce 6 nanomicelles with high labeling yields and excellent *in vivo* serum stability. After intravenous injection (*i.v.*) into tumor-bearing mice, ultra-high efficient passive tumor accumulation of PEG-Ce 6 nanomicelles was observed, attributed to the EPR effect elicited by most solid tumors. *In vivo* PDT was carried out in a mouse tumor model by *i.v.* injection of PEG-Ce 6 nanomicelles and a low power density of laser irradiation of tumors, achieving an excellent therapeutic efficacy. Therefore, our work presented a simplified approach to fabricate biocompatible multifunctional PEG-Ce 6-based theranostic agents with great translational potential for multimodality image-guided cancer therapy.

Results and discussion

PEG-Ce 6 nanomicelles were synthesized by conjugating Ce 6 molecules to the amine groups on the C_{18}PMH-PEG-NH_2 polymer through amide coupling using our previous procedures with slight modifications[38, 43] (Figure 1a). The maleic anhydride groups of the poly(maleic anhydride-*alt*-1-octadecene) (C_{18}PMH) backbone were reacted with the primary Boc-protected amine-terminated poly(ethylene glycol) methyl ethers (Boc-NH-mPEG_{3350}-NH_2). The remaining carboxylic acids of C_{18}PMH were then coupled to additional mPEG_{5000}-NH_2 *via* EDC-mediated amide formation to obtain a fully PEGylated polymer. Next, trifluoroacetic acid (TFA) was used to remove the protected Boc group to yield highly water soluble amphiphilic polymer-containing amine group (C_{18}PMH-PEG-NH_2). The Ce 6 molecules were then conjugated to the amine groups of C_{18}PMH-PEG-NH_2 polymer (Detail synthesis procedure were seen from experimental section). In order to accurately quantify the reaction efficiency, a ninhydrin-based assay was used to quantify the -NH_2 group in each step.[44] In the ninhydrin-based assay, ninhydrin reacts with the primary amine to generate a

chromophore in deep blue or purple color, known as Ruhemann's purple. After the first conjugation, 31.02% of -NH_2 was left of the C_{18}PMH-PEG-NH_2 polymer for conjugating Ce 6 molecules. In the next reaction, ~24.93 % of Ce 6 molecules was conjugated to the whole polymer (Table S1). ^{1}H nuclear magnetic resonance (NMR) spectra also reflected the -NH_2 group changing at different synthetic steps (Supporting Figure S1).

Transmission electron microscopy (TEM) image revealed that the nanomicelles were spherical with a size of ~20 nm (Figure 1b), agreeing with their hydrodynamic sizes measured by dynamic light scattering (DLS, Figure 1c). The formed PEG-Ce 6 nanomicelles were highly stable in various physiological solutions, without showing any aggregation in PBS or FBS salt solutions (Figure 1c, inset). Unlike Ce 6 molecules loaded in nanomaterials by physical adsorption that tended to detach from the system, our PEG-Ce 6 nanomicelles were stable for at least a week, suggesting that they could be used as a good drug delivery system (Supporting Figure S2). UV-Vis-NIR spectrum revealed the characteristic peaks of Ce 6 (404 nm and 650 nm) for PEG-Ce 6 nanomicelles (Figure 1d). From the spectrum, ~25.17% of the Ce 6 molecules were conjugated to the polymer, which validated the findings from the ninhydrin-based assay. Ce 6 is widely used photosensitizer for photodynamic cancer therapy and could effectively generate singlet oxygen under light irradiation. Compared with free Ce 6, PEG-Ce 6 nanomicelles (Ce 6 concentration of 0.1 mg/mL) showed similar efficiency of light-triggered singlet oxygen production at the same Ce 6 concentrations (Figure 1e), indicating that the synthesized PEG-Ce 6 nanomicelles could be used as a high-performance PDT agent. After putting PEG-Ce 6 nanomicelles in 1% sodium dodecyl sulfate (SDS) solution, we did not find any noticeable quenching effect (Supporting Figure S3), also indicating that most of the Ce 6 molecules were conjugated onto the surface of the nanomicelles.

To explore the applications of PEG-Ce 6 nanomicelles in biomedicine, we first tested their potential toxicity to several types of cells. The standard methyl thiazolyl tetrazolium (MTT) assay was carried out to determine the relative viabilities of NIH3T3 (mouse fibroblast cell line), HaCaT (human keratinocyte cell line), 4T1 murine breast cancer cells, U87MG human glioblastoma cells, and MDA-MB-231 breast carcinoma cells. After incubating with PEG-Ce 6 nanomicelles at various concentrations for 24 h, no significant cell cytotoxicity of PEG-Ce 6 nanomicelles was observed even at high concentrations up to 10 μM (Supporting Figure S4). The intracellular behavior of our PEG-Ce 6 nanomicelles after endocytosis was also investigated. 4T1 cells were incubated with PEG-Ce 6 nanomicelles for different periods of time and imaged with a confocal microscope (Figure 2). From the images, we observed Ce 6 signal inside cells after 3 h incubation, which increased as prolonging of incubation time. The PDT effect is strongly dependent on the uptake of photosensitizers by tumor cells. Next, we used PEG-Ce 6 nanomicelles as the photodynamic agent for *in vitro* cancer therapy under laser irradiation. 4T1 cells were incubated with various concentrations of PEG-Ce 6 nanomicelles for 24 h and then irradiated by the 658-nm laser. After that, the cells were cultured for another 12 h. MTT assay was performed to quantify the relative cell viabilities after PDT treatment (Figure 3a, Supporting Figure S5). A dose and laser power density-dependent cellular toxicity was observed. The majority of cells were destroyed after incubation with 5 μM of PEG-Ce 6 nanomicelles and exposure to the 658 nm laser with power density of 20 mW/cm^2 for 15 min. In contrast, the control group (cells incubated

without PEG-Ce 6 nanomicelles) was not affected under the same laser irradiation. The PDT effects of PEG-Ce 6 nanomicelles on 4T1 cells were further investigated using Trypan blue staining. Cells in the control groups showed no color, confirming that laser irradiation alone or PEG-Ce 6 nanomicelles incubated alone was not harmful to the cells. Upon laser irradiation, most cells incubated with PEG-Ce 6 nanomicelles were killed, as indicated by the intense homogeneous blue color (Figure 3b). The amount of cell death gradually increased upon increasing the concentrations of PEG-Ce 6 nanomicelles, which was consistent with the MTT results. These findings all together revealed that PEG-Ce 6 nanomicelles hold great promise as an effective photodynamic agent for *in vivo* tumor therapy.

The porphyrin structure of Ce 6 has the intrinsic ability to chelate a variety of metal ions, such as Cu^{2+}, Gd^{3+}, and Mn^{2+}, by forming stable complexes.[35, 38, 39] In this work, we used the porphyrin ring of Ce 6 to chelate $^{64}Cu^{2+}$, which could be used as a highly sensitive PET imaging probe. By mixing $^{64}CuCl_2$ with PEG-Ce 6 nanomicelles at 37 °C for 1 h under constant shaking, we found that $^{64}Cu^{2+}$ was immediately adsorbed by PEG-Ce 6 nanomicelles (^{64}Cu-PEG-Ce 6) as detected by thin-layer chromatography (TLC) and the labeling yield was measured to be as high as 90% after 1 h of incubation (Figure 4a, Supporting Figure S6). Moreover, the ^{64}Cu labeling of ^{64}Cu-PEG-Ce 6 nanomicelles was highly stable in mouse serum for 48 h, even in a 1,4,7-triazacyclononane-1,4,7-triacetic acid (NOTA) competitive situation (Figure 4b, Supporting Figure S7).

Such highly efficient and stable chelator-free labeling of ^{64}Cu-PEG-Ce 6 nanomicelles would be suitable for *in vivo* PET imaging. 4T1 tumor-bearing mice were imaged using a microPET Inveon rodent model scanner at various time points post *i.v.* injection of ^{64}Cu-PEG-Ce 6 nanomicelles (~10 MBq). Interestingly, the nanomicelles showed an efficient time-dependent tumor accumulation after injection (Figure 4c). Quantitative data obtained from region-of-interest (ROI) analysis of these PET images revealed that the tumor uptakes of ^{64}Cu-PEG-Ce 6 nanomicelles were determined to be 2.5 ± 0.4, 4.4 ± 0.8, 6.7 ± 1.4, 8.3 ± 1.3, 11.6 ± 1.7, and 13.7 ± 2.2 %ID/g at 0.5h, 3 h, 6 h, 16 h, 24 h, and 48 h post-injection (p.i.), respectively (n = 3; Figure 4d). The values were much higher than the previously reported PDT agents[36, 38, 45, 46]. Moreover, the tumor-to-muscle (T/M) ratio increased over time as well. Even at the later time points, a high signal in the heart suggested a long blood circulation time for the nanomicelles. Such an efficient passive tumor homing of the nanomicelles could be attributed to the EPR effect of 4T1 tumors. To further confirm the accuracy of PET quantification analysis, *ex vivo* biodistribution studies were carried out at 24 h and 48 h p.i.. As shown in Figure 4e, the tumor uptake at 48 h p.i. was a slightly higher than that at 24 h post injection with values of 9.8 ± 1.6%ID/g and 10.85 ± 1.4%ID/g for 24 h and 48 h respectively (n = 3). The quantitative results based on PET and biodistribution studies were consistent indicating that serial non-invasive PET imaging accurately reflected the distribution of PEG-Ce 6 nanomicelles in 4T1 tumor-bearing mice. In addition, we found the signals in liver decreased from 27.5 ± 0.4 %ID/g to 16.2 ± 0.7 %ID/g (Figure 4d) suggesting that part of PEG-Ce 6 nanomicelles could be excreted from the body over time. In order to further confirm this, ^{64}Cu-PEG_{5K}-Ce 6 polymer was conjugated by the same method and *i.v.* injected into mice for PET imaging (Supporting Figure S8). Most of the polymer cleared from the body and displayed low tumor retention after 24 h, which was

different from the result of PEG-Ce 6 nanomicelles. However, more detailed studies are still required in the future to systematically examine the clearance and potential long-term toxicity of PEG-Ce 6 nanomicelles in animals to enable further support for this new type of photosensitizer-based nanomicelles in biomedicine.

In vivo fluorescence (FL) imaging was also conducted at different time points after injection of PEG-Ce 6 nanomicelles. The fluorescence signal from the PEG-Ce 6 nanomicelles increased in the tumor over time, with prominent uptake of the nanomicelles observed in the tumor at 24 h p.i. (Figure 5a&b). *Ex vivo* imaging at 24 h p.i. revealed that Ce 6 fluorescence signals were mainly in liver, spleen, and tumor tissues (Figure 5c). To confirm the accumulation of PEG-Ce 6 nanomicelles in tumor, tumor tissues were sectioned and imaged by confocal microscopy. As shown in Figure 5d, strong red fluorescence were clearly visualized in tumor sections, verifying the prominent uptake of PEG-Ce 6 nanomicelles in the tumor at 24 h p.i.. However, there was no fluorescence signal detected from the tumor devoid of nanomicelles when using the same imaging conditions. The results clearly showed the efficient tumor passive uptake of our PEG-Ce 6 nanomicelles, which was consistent with the imaging results.

From the above results, our synthesized PEG-Ce 6 nanomicelles could be successfully used as a PET/FL dual-modal imaging contrast agent. Each imaging modality has its own unique advantages along with intrinsic limitations.[47–49] The main advantages of PET imaging are their high sensitivity and lack of tissue penetrating limit, allowing for the identification of cancerous tissues at early disease stages and sensitive assessment of malignant *versus* normal tissues. While effective, PET imaging does not provide anatomical information.[41, 50] The advantages of optical imaging includes its high sensitivity, multicolor imaging capabilities and no requirement of radioactivity, yet this imaging modality lacks the high spatial resolution and poor tissue penetration needed for clinical translation at this time.[47] As a means to solve these problems, multimodality imaging is a powerful technique that can provide more reliable and accurate detection of diseased sites. PET imaging would be able to qualify the tumor retention of nano-agents in real-time, while FL imaging could then be used in a variety of ways to validate, correlate, or add new information to the observations of the other modalities at low cost and possibly on a cellular or molecular level. Most importantly, our PEG-Ce 6 nanomicelles could also chelate Mn^{2+} or Gd^{3+} for additional magnetic resonance imaging, which provides high-resolution images for anatomical information. Therefore, the combination of those different imaging modalities (PET/FL/MRI) would be of great importance to provide valuable information with high sensitivity and high resolution, helping physicians design better therapeutic approaches for the treatment of cancer.

Encouraged by the high tumor accumulation of PEG-Ce 6 nanomicelles and strong capability to induce *in vitro* PDT, we performed *in vivo* PDT experiments to confirm the efficacy of the nanomicelles. Four mice bearing 4T1 tumors with the average size of ~ 150 mm^3 on their back were *i.v.* injected with PEG-Ce 6 nanomicelles (200 μL, 1 mg/mL). At 24 h *p.i.*, each tumor was exposed to the 658-nm laser at a power density of 50 mW/cm^2 for 30 min. Three other groups including untreated mice (Control, n=4), mice exposed to the laser (Laser only, n=4), and PEG-Ce 6 nanomicelles injected mice without laser irradiation (PEG-

Ce 6, n = 4), were used as the controls (with the average tumor volume at ~60 mm^3). Tumor sizes were measured every two days after treatment. Remarkably, tumor growth in PEG-Ce 6 injected mice was completely inhibited after NIR laser irradiation (Figure 6a). In contrast, neither laser irradiation alone nor PEG-Ce 6 nanomicelles injection without irradiation affected the tumor growth (Figure 6b&6c, Supporting Figure S9). These results suggested that PEG-Ce 6 nanomicelles were a powerful agent for *in vivo* PDT of cancer. In order to further understand the PDT effects after various treatments down to the cellular level, hematoxylin and eosin (H&E) staining was introduced to study the morphology and apoptosis of tumor cells after 2 days post-treatment. The results indicated that most cancer cells were completely destroyed in the PEG-Ce 6 nanomicelles with laser treatment group, while cells in the other three control groups partly or mainly retained their normal morphology (Figure 6d) further confirming the efficacy of PEG-Ce 6 nanomicelles for *in vivo* photodynamic ablation of cancer.

Conclusions

In summary, PEG-Ce 6 nanomicelles were successfully synthesized and used for PET/FL dual-modal image guided photodynamic cancer therapy. By a simple conjugation, PEG-Ce 6 nanomicelles with uniform size of ~20 nm exhibited excellent stability and compatibility in various physiological solutions. Due to the porphyrin structure of Ce 6 molecules, the synthesized PEG-Ce 6 nanomicelles served as a good chelating agent to label $^{64}Cu^{2+}$ for PET imaging. ^{64}Cu could chelate on the surface of PEG-Ce 6 nanomicelles with great labeling yield and high *in vivo* serum stability. Ultra-high efficient passive tumor accumulation of PEG-Ce 6 nanomicelles *via* EPR effect was visualized based on PET/FL dual-modal imaging after *i.v.* injection into the mice. Finally, *in vivo* PDT was carried out in a mouse tumor model by *i.v.* injection of PEG-Ce 6 nanomicelles and a low power density of laser irradiation to tumors was shown to achieve an excellent therapeutic efficacy. The work presented in this study elaborated a simple approach to fabricate biocompatible multifunctional PEG-Ce 6-based theranostic agents with great potential for multimodality imaging-guided tumor therapy. The small size of nanoparticles or nanomicelles allows for partial renal clearance and high tumor uptake behavior *in vivo*, which will improve future applications and potential clinical translation of these theranostic agents.

Methods/Experimental

Materials

Poly (maleic anhydride-alt-1-octadecene) (C_{18}PMH), 1-ethyl-3-(3-(dimethylamino) -propyl)carbodimide (EDC), and Sulfo-NHS (N-hydroxysulfosuccinimide) were obtained from Sigma-Aldrich. Chlorine e6 (Ce 6) were from J&K Chemical Co. Dimethyl sulfoxide (DMSO) and trifluoroacetic acid (TFA) were obtained from Sinopharm Chemical Reagent Co. mPEG-NH_2 (5k), and Boc-PEG-NH_2(3350) were obtained from Biomatrik Co., Ltd (Jiaxing, China). Deionized water used in our experiments was obtained from a Milli-Q water system.

Synthesis of C_{18}PMH-PEG-NH_2 polymer

C_{18}PMH-PEG-Ce 6 polymer was synthesized according to the protocol reported previously with sight modification.[38, 43] 10 mg C_{18}PMH was mixed with 96 mg Boc-PEG-NH_2 (3350) in 3 mL dichloromethane to render a transparent solution. After adding 6 μL TEA and 6 mg EDC, the solution was stirred for overnight. Then, 143 mg mPEG-NH_2 (5k) and 6 mg EDC predissolved in 2 mL dichloromethane was added to the above solution. After stirring for another 24 h, the dichloromethane solvent was dried under N_2. Subsequently, 4 mL TFA was added under magnetic stirring for another 4 h at room temperature to de-protect the Boc group. After evaporating the TFA solvent, the solid was dissolved in water and dialyzed for two days in a dialysis bag (MWCO 14 kDa) to remove unreacted PEG polymers and other reagents. After lyophilization, the final product (C_{18}PMH-PEG-NH_2) in white solid was stored at −20°C for future use.

Synthesis of PEG-Ce 6 nanomicelles

The Ce 6 conjugated C_{18}PMH-PEG (C_{18}PMH-PEG-Ce 6) was prepared by conjugating the amine-functionalized C_{18}PMH-PEG-NH_2 with activated Ce 6. Briefly, 17 mg of Ce 6 was mixed with 15 mg EDC and 15 mg Sulfo-NHS in 4 mL anhydrous DMSO for 1 h at room temperature. 50 mg of C_{18}PMH-PEG-NH_2 in 4 ml DMSO was added afterwards (molar ratio of PEG-NH_2 : Ce 6 : EDC : NHS=1:2:5:5). After reacting for 24 h at room temperature, the above solution was dialyzed against water by a 14 KDa cut-off membrane and then lyophilized to obtain PEG-Ce 6 nanomicelles. All polymers and nanomicelles obtained at each step were analyzed by ^{1}H nuclear magnetic resonance (NMR).

Quantification of NH_2 groups using ninhydrin-based assay

All reagents used for the assay were prepared according to the literature.[44] Typically, a 6% ninhydrin ethanol solution was prepared by dissolving 2.5 g of ninhydrin in 50 mL of anhydrous ethanol. The KCN pyridine solution and 80% phenol solution in ethanol from the Kaiser test kit were combined at a 1:1 volume ratio to give a KCN/phenol solution. Briefly, 200 μL of 6% ninhydrin ethanol solution and 400 μL of KCN/phenol solution were added to each 2 mL of C_{18}PMH-PEG-NH_2 (150 mg) or PEG-Ce 6 nanomicelle (100 mg) solutions, followed by heating at 100 °C for 5 min. After being cooled in an ice bath, 2.4 mL of 60 wt % ethanol in water was added. UV-vis spectra were then recorded at 570 nm. A negative control with all agents, but no polymers or nanomicelles, was used as the baseline. The -NH_2 on C_{18}PMH-PEG-NH_2 or PEG-Ce 6 nanomicelles were calculated using the following equation. Each data point represents an average of three replicas.

$$\mathrm{NH_2\ concentration\ (nmol/mL)} = [(\mathrm{IAbs_{sample}} - \mathrm{IAbs_{baseline}}) * 5 * 1000/15000] * 1000$$

Characterization

Transmission electron microscopy (TEM) images of the nanomicelles were obtained using a FEI Tecnai F30 transmission electron microscope at an acceleration voltage of 300 kV. UV-vis-NIR spectra were obtained with PerkinElmer Lambda 750 UV-vis-NIR spectrophotometer. Fluorescence spectra of different samples were obtained on a FluoroMax

4 luminescence spectrometer (HORIBA Jobin Yvon). The hydrodynamic diameters of PEG-Ce 6 nanomicelles were determined by a ZetaSizer Nano-ZS (Malvern Instruments, UK).

Single oxygen detection

The method for singlet oxygen detection was based on the protocol reported previously.[51] In brief, 100 mg of SOSG (Molecular Probes, USA) was dissolved in 330 mL of methanol to obtain the stock solution of SOSG (0.5 mM). Then, 10 μL of SOSG was added to 2 mL of PEG-Ce 6 nanomicelles solution containing 1 μM Ce 6. Next, the sample was irradiated by a 658 nm laser at a power density of 20 mW/cm^2. The same concentration of free Ce 6 molecules under laser irradiation was used as the control. The fluorescence intensity of SOSG was measured with an excitation wavelength of 494 nm.

Cell culture experiment

Mouse fibroblast cells (NIH3T3), human keratinocyte cells (HaCaT), Murine breast cancer cells (4T1), human glioblastoma cells (U87MG), and breast carcinoma cells (MDA-MB-231) were obtained from American Type Culture Collection (ATCC) and cultured at 37 °C under 5% CO_2. All cell culture related reagents were purchased from Invitrogen. 4T1 cells and MB-231 cells were cultured in normal RPMI-1640 medium containing 10% fetal bovine serum (FBS) and 1% penicillin/streptomycin. NIH3T3, HaCaT, and U87MG cells were cultured in DMEM low-glucose medium containing 10% fetal bovine serum and 1% penicillin/streptomycin. Cells were seeded into 96-well plates at a density of 1×10^4 cells per well and incubated with different concentrations of PEG-Ce 6 nanomicelles for 24 h. Relative cell viabilities were determined by the standard methyl thiazolyl tetrazolium (MTT) assay.

To examine the cellular uptake of PEG-Ce 6 nanomicelles, 4T1 cells were plated in 6-well plates at 1×10^6 cells per well. After adhesion, PEG-Ce 6 nanomicelles were added into the wells at the concentration of 5 μM (Ce 6) and cultured for different time periods (3 h, 6 h, 12 h, and 24 h). After washing three times with PBS (pH = 7.4), cells were cells were fixed by 75% ethanol and labeled with 4′, 6-diamidino-2-phenylindole (DAPI) before imaging with a Nikon Digital Eclipse C1 plus microscope.

In vitro photodynamic therapy

For *in vitro* PDT, 4T1 cells (1×10^4) were seeded in 96-well plates and added with PEG-Ce 6 nanomicelles at various concentrations. After incubation for 12 h, the experimental groups were exposed to 658 nm laser irradiation under a power density of 20 mW/cm^2 for 15 min, while the control groups were still cultured in dark. Afterwards, all samples were incubated in the dark for another 12 h. In order to determine relative cell viabilities after various treatments, the MTT assay was carried out following the standard protocol. After laser irradiation, cells were washed with PBS and stained with 0.4% Trypan blue (Sigma) before imaged by a Nikon Elipse Ti microscope.

Tumor models

All animal studies were conducted under a protocol approved by the University of Wisconsin Institutional Animal Care and Use Committee. The 4T1 subcutaneous xenografts

were generated by subcutaneous injection of 1×10^6 cells in ~30 μL RMPI-1640 medium onto the back of each female Balb/c mice. In order to investigate the optical imaging of polymer-Ce 6 nanomicelles, female nude mice were employed. To develop the tumor model, 1×10^6 cells in a 1:1 ratio of PBS to Corning Matrigel (Corning Inc., USA) medium were injected onto the back of female nude athymic mice. The mice were used when tumor volumes reached about ~70 mm^3.

^{64}Cu labeling and animal modal for PET imaging

^{64}Cu was produced with an onsite cyclotron (GE PETtrace). Briefly, $^{64}CuCl_2$ (~150 MBq) was diluted in 300 μL of 0.1 M sodium acetate buffer (pH 5.5) and mixed with 100 μL of PEG-Ce 6 nanomicelles (0.2 mg/mL). The reaction was conducted at 37°C for 60 min with constant shaking. The labeling yield was determined by thin-layer chromatography (TLC) at different time points. The resulting ^{64}Cu-PEG-Ce 6 was purified using PD-10 columns with PBS as the mobile phase.

The serum stability study was carried out to ensure ^{64}Cu was stably attached on PEG-Ce 6 nanomicelles. ^{64}Cu-Ce 6-PEG was incubated in PBS and complete serum at 37 °C for up to 24 h. At different time points, portions of the mixture were sampled and filtered through 300-kDa MWCO filters. The retained (*i.e.,* intact) ^{64}Cu on ^{64}Cu-PEG-Ce 6 nanomicelles was calculated using the equation (radioactivity on filter/total sampled radioactivity × 100%)

NOTA Challenge Study

To demonstrate the stability of ^{64}Cu-PEG-Ce 6 nanomicelles, 20 μL of 1 mM 1,4,7-triazacyclononane-1,4,7-triacetic acid (NOTA) was added to 250 μL of ^{64}Cu-PEG-Ce 6 nanomicelles (~300 μCi) in complete mouse serum (pH = 7) at 37 °C under constant shaking (550 rpm) for 48 h. At each time point, 25 μL of the mixture was taken out and resuspended in 100 μL of NaOAc buffer. A 300-kDa filter was used to separate potential ^{64}Cu-NOTA from ^{64}Cu-PEG-Ce 6 nanomicelles. The radioactivity of ^{64}Cu-NOTA and ^{64}Cu-PEG-Ce 6 nanomicelles was measured using a gamma counter (PerkinElmer).

For PET imaging, 4T1 tumor-bearing mice (3 mice per group) post *i.v* injection of ~10 MBq of ^{64}Cu-PEG-Ce 6 nanomicelles solution were imaged using a microPET/microCT Inveon rodent model scanner (Siemens Medical Solutions USA, Inc.). Data acquisition, image reconstruction, and ROI analysis of the PET data were performed as described previously.[52] After the PET scans at 24 h and 48 h p.i., *ex vivo* biodistribution studies were carried out to ensure the %ID/g values determined by PET imaging truly represented the radioactivity distribution in tumor-bearing mice. Mice were euthanized, and blood, tumor, and major organs/tissues were collected and wet-weighed. The radioactivity in the tissue was measured using a gamma-counter (PerkinElmer, USA) and presented as %ID/g (mean ±SD).

In vivo fluorescence imaging of PEG-Ce 6 nanomicelles

For *in vivo* imaging, 200 μL of PEG-Ce 6 nanomicelles with 0.5 mg/mL Ce 6 was *i.v.* injected into each mouse. *In vivo* fluorescence imaging was conducted using an IVIS Spectrum *in vivo* fluorescence imager. Mice were then imaged using a 675 nm/740 nm excitation/emission filter pair under automatic exposure settings, and fluorescence signal

was displayed as radiant efficiency. The mice were sacrificed 24 h after *i.v.* injection, with their major organs including the tumor, liver, heart, lung, spleen, and kidneys collected for *ex vivo* imaging. Lastly, the tumor tissues were frozen in optimum cutting temperature (OCT) compound (SACURA, USA) medium and cut into 8 μm slices for confocal imaging.

In vivo PDT

To develop the tumor model, 4T1 cells (1×10^6) suspended in 30 μL of PBS were subcutaneously injected into the back of each BALB/c mouse. After the tumor volume reached ~150 mm^3, mice were randomly divided into four groups (n = 4 per group) for various treatments: (i) Control; (ii) Laser only; (iii) PEG-Ce 6 nanomicelles *i.v.* injection; and PEG-Ce 6 nanomicelles *i.v.* injection + Laser. PEG-Ce 6 nanomicelles, at a dose of 10 mg/kg, were *i.v.* injected into mice bearing 4T1 tumors. PDT treatments were conducted 24 h later, with the 658-nm laser at the power density of 50 mW/cm^2 for 30 min. The tumor sizes were measured by a caliper every the other day and calculated as the volume = (tumor length) × (tumor width)^2/2. Relative tumor volumes were calculated as V/V_0 (V_0 was the initial tumor volume). Two days after treatment, the tumors in each group were dissected to make paraffin sections for further hematoxylin and eosin (H&E) staining.

Supplementary Material

Refer to Web version on PubMed Central for supplementary material.

Acknowledgments

This work was supported by the National Natural Science Foundation of China (51302180, 51572180), the Post-doctoral science foundation of China (2013M531400, 2014T70542). L. Cheng also acknowledges the Collaborative Innovation Center of Suzhou Nano Science and Technology (Nano-CIC) for the fellowship of “Young Scientists Overseas Exchanges And Cooperation Program”. This work was also partly supported by the University of Wisconsin-Madison, the National Institutes of Health (NIBIB/NCI 1R01CA169365, P30CA014520, and T32CA009206), and the American Cancer Society (125246-RSG-13-099-01-CCE). We thank Linchao Zhu from department of Chemistry (University of Wisconsin-Madison) for NMR characterization, and this work was supported by Office of the Director, National Institutes of Health under award number (S10OD012245).

References

1. Bardhan R, Lal S, Joshi A, Halas NJ. Theranostic Nanoshells: From Probe Design to Imaging and Treatment of Cancer. Acc Chem Res. 2011; 44:936–946. [PubMed: 21612199]
2. http://www.thelancet.com/journals/lancet/article/PIIS0140-6736(03)13038-3/abstract.
3. Paltauf G, Dyer PE. Photomechanical Processes and Effects in Ablation. Chem Rev. 2003; 103:487–518. [PubMed: 12580640]
4. Cheng L, Wang C, Feng L, Yang K, Liu Z. Functional Nanomaterials for Phototherapies of Cancer. Chem Rev. 2014; 114:10869–10939. [PubMed: 25260098]
5. Dolmans DEJGJ, Fukumura D, Jain RK. Photodynamic Therapy for Cancer. Nat Rev Cancer. 2003; 3:380–387. [PubMed: 12724736]
6. Moore CM, Pendse D, Emberton M. Photodynamic Therapy for Prostate Cancer: A Review of Current Status and Future Promise. Nat Clin Pract Urol. 2009; 6:18–30. [PubMed: 19132003]
7. Kamkaew A, Lim SH, Lee HB, Kiew LV, Chung LY, Burgess K. BODIPY Dyes in Photodynamic Therapy. Chem Soc Rev. 2013; 42:77–88. [PubMed: 23014776]
8. Zhen Z, Tang W, Chuang YJ, Todd T, Zhang W, Lin X, Niu G, Liu G, Wang L, Pan Z, Chen X, Xie J. Tumor Vasculature Targeted Photodynamic Therapy for Enhanced Delivery of Nanoparticles. ACS Nano. 2014; 8:6004–6013. [PubMed: 24806291]

9. Celli JP, Spring BQ, Rizvi I, Evans CL, Samkoe KS, Verma S, Pogue BW, Hasan T. Imaging and Photodynamic Therapy: Mechanisms, Monitoring, and Optimization. Chem Rev. 2010; 110:2795–2838. [PubMed: 20353192]
10. Ethirajan M, Chen Y, Joshi P, Pandey RK. The Role of Porphyrin Chemistry in Tumor Imaging and Photodynamic Therapy. Chem Soc Rev. 2011; 40:340–362. [PubMed: 20694259]
11. Hamblin MR, Miller JL, Rizvi I, Ortel B, Maytin EV, Hasan T. Pegylation of a Chlorin e6 Polymer Conjugate Increases Tumor Targeting of Photosensitizer. Cancer Res. 2001; 61:7155–7162. [PubMed: 11585749]
12. Lammers T, Aime S, Hennink WE, Storm G, Kiessling F. Theranostic Nanomedicine. Acc Chem Res. 2011; 44:1029–1038. [PubMed: 21545096]
13. Barnett BP, Arepally A, Karmarkar PV, Qian D, Gilson WD, Walczak P, Howland V, Lawler L, Lauzon C, Stuber M, Kraitchman DL, Bulte JWM. Magnetic Resonance-Guided, Real-time Targeted Delivery and Imaging of Magnetocapsules Immunoprotecting Pancreatic Islet Cells. Nat Med. 2007; 13:986–991. [PubMed: 17660829]
14. Shen J, Zhao L, Han G. Lanthanide-doped Upconverting Luminescent Nanoparticle Platforms for Optical Imaging-Guided Drug Delivery and Therapy. Adv Drug Delivery Rev. 2013; 65:744–755.
15. de Jong M, Essers J, van Weerden WM. Imaging Preclinical Tumour Models: Improving Translational Power. Nat Rev Cancer. 2014; 14:481–493. [PubMed: 24943811]
16. Cheng Y, Meyers JD, Broome AM, Kenney ME, Basilion JP, Burda C. Deep Penetration of a PDT Drug into Tumors by Noncovalent Drug-Gold Nanoparticle Conjugates. J Am Chem Soc. 2011; 133:2583–2591. [PubMed: 21294543]
17. Lin J, Wang S, Huang P, Wang Z, Chen S, Niu G, Li W, He J, Cui D, Lu G, Chen X, Nie Z. Photosensitizer-Loaded Gold Vesicles with Strong Plasmonic Coupling Effect for Imaging-Guided Photothermal/Photodynamic Therapy. ACS Nano. 2013; 7:5320–5329. [PubMed: 23721576]
18. Zhang Y, Qian J, Wang D, Wang Y, He S. Multifunctional Gold Nanorods with Ultrahigh Stability and Tunability for *In Vivo* Fluorescence Imaging, SERS Detection, and Photodynamic Therapy. Angew Chem Int Ed. 2013; 52:1148–1151.
19. Tian B, Wang C, Zhang S, Feng L, Liu Z. Photothermally Enhanced Photodynamic Therapy Delivered by Nano-Graphene Oxide. ACS Nano. 2011; 5:7000–7009. [PubMed: 21815655]
20. Huang P, Lin J, Wang X, Wang Z, Zhang C, He M, Wang K, Chen F, Li Z, Shen G, Cui D, Chen X. Light-Triggered Theranostics Based on Photosensitizer-Conjugated Carbon Dots for Simultaneous Enhanced-Fluorescence Imaging and Photodynamic Therapy. Adv Mater. 2012; 24:5104–5110. [PubMed: 22718562]
21. Ge J, Lan M, Zhou B, Liu W, Guo L, Wang H, Jia Q, Niu G, Huang X, Zhou H, Meng X, Wang P, Lee CS, Zhang W, Han X. A Graphene Quantum Dot Photodynamic Therapy Agent with High Singlet Oygen Generation. Nat Commun. 2014; 5:4596. [PubMed: 25105845]
22. Coll C, Bernardos A, Martínez-Máñez R, Sancenón F. Gated Silica Mesoporous Supports for Controlled Release and Signaling Applications. Acc Chem Res. 2013; 46:339–349. [PubMed: 23214509]
23. Zhang C, Zhao K, Bu W, Ni D, Liu Y, Feng J, Shi J. Marriage of Scintillator and Semiconductor for Synchronous Radiotherapy and Deep Photodynamic Therapy with Diminished Oxygen Dependence. Angew Chem Int Ed. 2015; 127:1790–1794.
24. Idris NM, Gnanasammandhan MK, Zhang J, Ho PC, Mahendran R, Zhang Y. *In Vivo* Photodynamic Therapy Using Upconversion Nanoparticles as Remote-Controlled Nanotransducers. Nat Med. 2012; 18:1580–1585. [PubMed: 22983397]
25. Wang C, Tao H, Cheng L, Liu Z. Near-Infrared Light Induced *In Vivo* Photodynamic Therapy of Cancer based on Upconversion Nanoparticles. Biomaterials. 2011; 32:6145–6154. [PubMed: 21616529]
26. Nomoto T, Fukushima S, Kumagai M, Machitani K, Arnida, Matsumoto Y, Oba M, Miyata K, Osada K, Nishiyama N, Kataoka K. Three-Layered Polyplex Micelle as A Multifunctional Nanocarrier Platform for Light-Induced Systemic Gene Transfer. Nat Commun. 2014; 5:3545. [PubMed: 24694458]
27. Van Nostrum CF. Polymeric Micelles to Deliver Photosensitizers for Photodynamic Therapy. Adv Drug Delivery Rev. 2004; 56:9–16.

28. Elsabahy M, Heo GS, Lim SM, Sun G, Wooley KL. Polymeric Nanostructures for Imaging and Therapy. Chem Rev. 2015; 115:10967–11011. [PubMed: 26463640]
29. Huang YY, Sharma SK, Dai T, Chung H, Yaroslavsky A, Garcia-Diaz M, Chang J, Chiang LY, Hamblin MR. Can Nanotechnology Potentiate Photodynamic Therapy? Nanotechnology Rev. 2012; 1:111–146.
30. Sheng Z, Hu D, Zheng M, Zhao P, Liu H, Gao D, Gong P, Gao G, Zhang P, Ma Y, Cai L. Smart Human Serum Albumin-Indocyanine Green Nanoparticles Generated by Programmed Assembly for Dual-Modal Imaging-Guided Cancer Synergistic Phototherapy. ACS Nano. 2014; 8:12310–12322. [PubMed: 25454579]
31. Kim CS, Tonga GY, Solfiell D, Rotello VM. Inorganic Nanosystems for Therapeutic Delivery: Status and Prospects. Adv Drug Delivery Rev. 2013; 65:93–99.
32. Yang ZY, Li H, Zeng YP, Hao YH, Liu C, Liu J, Wang WD, Li R. Photosensitizer-Loaded Branched Polyethylenimine-PEGylated Ceria Nanoparticles for Imaging-Guided Synchronous Photochemotherapy. ACS Appl Mater Interfaces. 2015; 7:24218–24228. [PubMed: 26485120]
33. Peer D, Karp JM, Hong S, Farokhzad OC, Margalit R, Langer R. Nanocarriers as An Emerging Platform for Cancer Therapy. Nat Nanotechnol. 2007; 2:751–760. [PubMed: 18654426]
34. Brigger I, Dubernet C, Couvreur P. Nanoparticles in Cancer Therapy and Diagnosis. Adv Drug Delivery Rev. 2012; 64:24–36.
35. Li Y, Lin T-y, Luo Y, Liu Q, Xiao W, Guo W, Lac D, Zhang H, Feng C, Wachsmann-Hogiu S, Walton JH, Cherry SR, Rowland DJ, Kukis D, Pan C, Lam KS. A Smart and Versatile Theranostic Nanomedicine Platform based on Nanoporphyrin. Nat Commun. 2014; 5:4712. [PubMed: 25158161]
36. Lovell JF, Jin CS, Huynh E, Jin H, Kim C, Rubinstein JL, Chan WCW, Cao W, Wang LV, Zheng G. Porphysome Nanovesicles Generated by Porphyrin Bilayers for Use as Multimodal Biophotonic Contrast Agents. Nat Mater. 2011; 10:324–332. [PubMed: 21423187]
37. Lovell JF, Liu TWB, Chen J, Zheng G. Activatable Photosensitizers for Imaging and Therapy. Chem Rev. 2010; 110:2839–2857. [PubMed: 20104890]
38. Gong H, Dong Z, Liu Y, Yin S, Cheng L, Xi W, Xiang J, Liu K, Li Y, Liu Z. Engineering of Multifunctional Nano-Micelles for Combined Photothermal and Photodynamic Therapy Under the Guidance of Multimodal Imaging. Adv Funct Mater. 2014; 24:6492–6502.
39. Chen Q, Wang X, Wang C, Feng L, Li Y, Liu Z. Drug-Induced Self-Assembly of Modified Albumins as Nano-theranostics for Tumor-Targeted Combination Therapy. ACS Nano. 2015; 9:5223–5233. [PubMed: 25950506]
40. Hou W, Xia F, Alves CS, Qian X, Yang Y, Cui D. MMP2-Targeting and Redox-Responsive PEGylated Chlorin e6 Nanoparticles for Cancer Near-Infrared Imaging and Photodynamic Therapy. ACS Appl Mater Interfaces. 2016; 8:1447–1457. [PubMed: 26638778]
41. Sun X, Cai W, Chen X. Positron Emission Tomography Imaging Using Radiolabeled Inorganic Nanomaterials. Acc Chem Res. 2015; 48:286–294. [PubMed: 25635467]
42. Sun X, Huang X, Guo J, Zhu W, Ding Y, Niu G, Wang A, Kiesewetter DO, Wang ZL, Sun S, Chen X. Self-Illuminating ^{64}Cu-Doped CdSe/ZnS Nanocrystals for *In Vivo* Tumor Imaging. J Am Chem Soc. 2014; 136:1706–1709. [PubMed: 24401138]
43. Cheng L, He W, Gong H, Wang C, Chen Q, Cheng Z, Liu Z. PEGylated Micelle Nanoparticles Encapsulating A Non-Fluorescent Near-Infrared Organic Dye as A Safe and Highly-Effective Photothermal Agent for *In Vivo* Cancer Therapy. Adv Funct Mater. 2013; 23:5893–5902.
44. Xia X, Yang M, Wang Y, Zheng Y, Li Q, Chen J, Xia Y. Quantifying the Coverage Density of Poly(ethylene glycol) Chains on the Surface of Gold Nanostructures. ACS Nano. 2012; 6:512–522. [PubMed: 22148912]
45. Kunjachan S, Pola R, Gremse F, Theek B, Ehling J, Moeckel D, Hermanns-Sachweh B, Pechar M, Ulbrich K, Hennink WE, Storm G, Lederle W, Kiessling F, Lammers T. Passive *versus* Active Tumor Targeting Using RGD- and NGR-Modified Polymeric Nanomedicines. Nano Lett. 2014; 14:972–981. [PubMed: 24422585]
46. Guo J, Hong H, Chen G, Shi S, Zheng Q, Zhang Y, Theuer CP, Barnhart TE, Cai W, Gong S. Image-Guided and Tumor-Targeted Drug Delivery with Radiolabeled Unimolecular Micelles. Biomaterials. 2013; 34:8323–8332. [PubMed: 23932288]

47. Rieffel J, Chitgupi U, Lovell JF. Recent Advances in Higher-Order, Multimodal, Biomedical Imaging Agents. Small. 2015; 11:4445–4461. [PubMed: 26185099]

48. Lee DE, Koo H, Sun IC, Ryu JH, Kim K, Kwon IC. Multifunctional Nanoparticles for Multimodal Imaging and Theragnosis. Chem Soc Rev. 2012; 41:2656–2672. [PubMed: 22189429]

49. Kim J, Piao Y, Hyeon T. Multifunctional Nanostructured Materials for Multimodal Imaging, and Simultaneous Imaging and Therapy. Chem Soc Rev. 2009; 38:372–390. [PubMed: 19169455]

50. Evangelista L, Zattoni F, Guttilla A, Saladini G, Zattoni F, Colletti PM, Rubello D. Choline PET or PET/CT and Biochemical Relapse of Prostate Cancer: A Systematic Review and Meta-Analysis. Clin Nucl Med. 2013; 38:305–314. [PubMed: 23486334]

51. Yang G, Gong H, Qian X, Tan P, Li Z, Liu T, Liu J, Li Y, Liu Z. Mesoporous Silica Nanorods Intrinsically Doped with Photosensitizers as A Multifunctional Drug Carrier for Combination Therapy of Cancer. Nano Res. 2014; 8:751–764.

52. Cheng L, Shen S, Shi S, Yi Y, Wang X, Song G, Yang K, Liu G, Barnhart TE, Cai W, Liu Z. $FeSe_2$-Decorated Bi_2Se_3 Nanosheets Fabricated *via* Cation Exchange for Chelator-Free ^{64}Cu-Labeling and Multimodal Image-Guided Photothermal-Radiation Therapy. Adv Funct Mater. 2016; 26:2185–2197. [PubMed: 27110230]

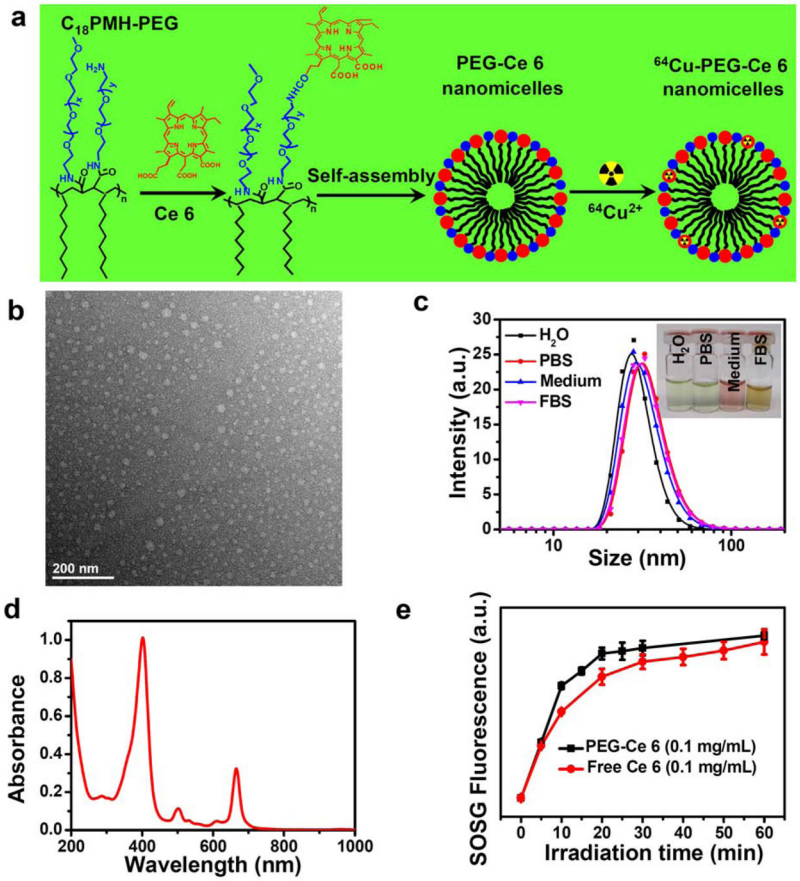

Figure 1.

Characterization of PEG-Ce 6 nanomicelles. (**a**) Scheme showing the synthesis of PEG-Ce 6 nanomicelles and chelate-free labeling $^{64}Cu^{2+}$ for PET imaging. (**b**) TEM image of PEG-Ce 6 nanomicelles. (**c**) DLS sizes of PEG-Ce 6 nanomicelles after being incubated in various physiological solutions for 24 h. Inset: a photograph of PEG-Ce 6 nanomicelles dispersed in water, PBS, cell culture medium and FBS. (**d**) UV-vis-NIR absorbance spectrum of PEG-Ce 6 nanomicelles in water. (**e**) Generation of singlet oxygen by measuring the fluorescence intensity changes of SOSG from PEG-Ce 6 nanomicelles and free Ce 6 molecules with the same concentration of Ce 6 (0.1 mg/mL). The increase of SOSG fluorescence was a result of singlet oxygen generation (n = 3).

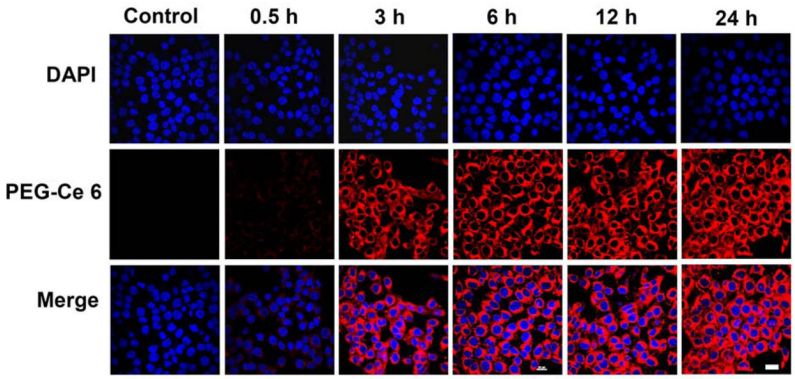

Figure 2.

Cellular internalization of PEG-Ce 6 nanomicelles. Confocal fluorescence images of 4T1 cells incubated with PEG-Ce 6 nanomicelles by recording Ce 6 fluorescence with different incubation times (0.5, 3, 6, 12, and 24 h). The scale bar is 20 μm.

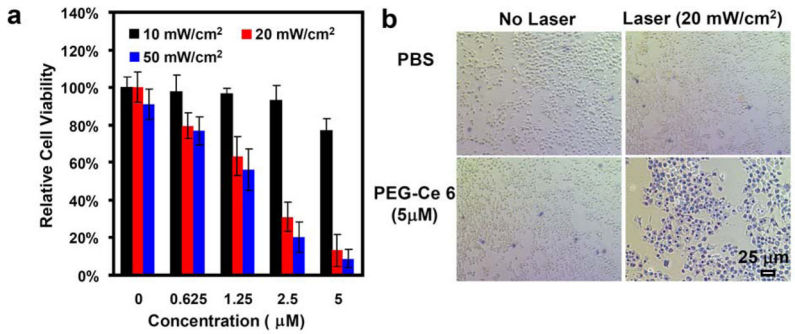

Figure 3.

In vitro PDT of PEG-Ce 6 nanomicelles. (**a**) Relative viabilities of 4T1 cells treated by PEG-Ce 6 nanomicelles under 658 nm light exposure with various power density for 15 min. n = 4. (**b**) Trypan blue stained 4T1 cells with PBS or PEG-Ce 6 nanomicelles incubation after being exposed to the 658 nm laser, with blue indicating dead cells.

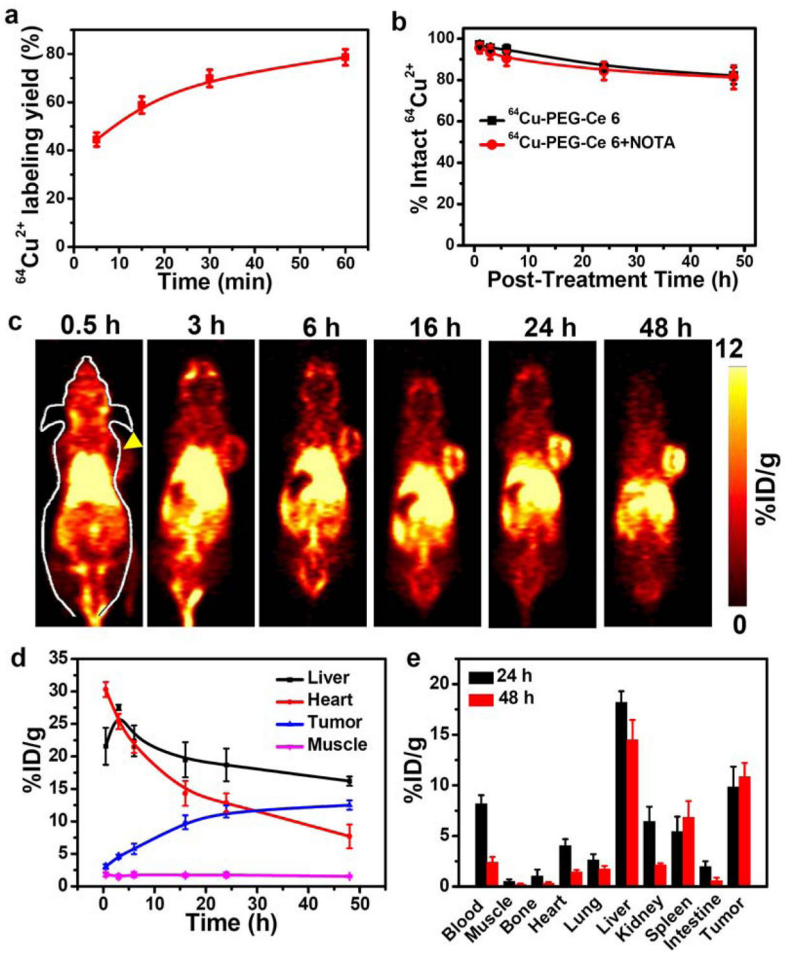

Figure 4.

In vivo PET imaging of ^{64}Cu-labeled PEG-Ce 6 nanomicelles. (**a**) Quantified labeling yield of ^{64}Cu on PEG-Ce 6 nanomicelles at various time points after incubation (n = 3). (**b**) Stability test of ^{64}Cu labeling on PEG-Ce 6 nanomicelles after incubation in serum with or without NOTA competitive reaction at 37 °C for different periods of time. Error bars were based standard deviations (SD) of three samples at each time point. (**c**) PET images of 4T1 tumor-bearing mice taken at various time points (0.5, 3, 6, 16, 24, and 48 h) post *i.v.* injection of ^{64}Cu-PEG-Ce 6 nanomicelles. Tumors are indicated by yellow arrowheads. (**d**) Quantification of ^{64}Cu-PEG-Ce 6 nanomicelles uptake in the liver, blood, 4T1 tumor, and muscle at various time points p.i.. The unit is the percentage of injected dose per gram of tissue (%ID/g). n = 3. (**e**) Biodistribution of PEG-Ce 6 nanomicelles at 24 and 48 h after *i.v.* injection into 4T1 tumor-bearing mice as determined by ^{64}Cu radioactivity measurement in various organs and tissues. Error bars were based on the standard error of the mean (SEM) of triplicate samples.

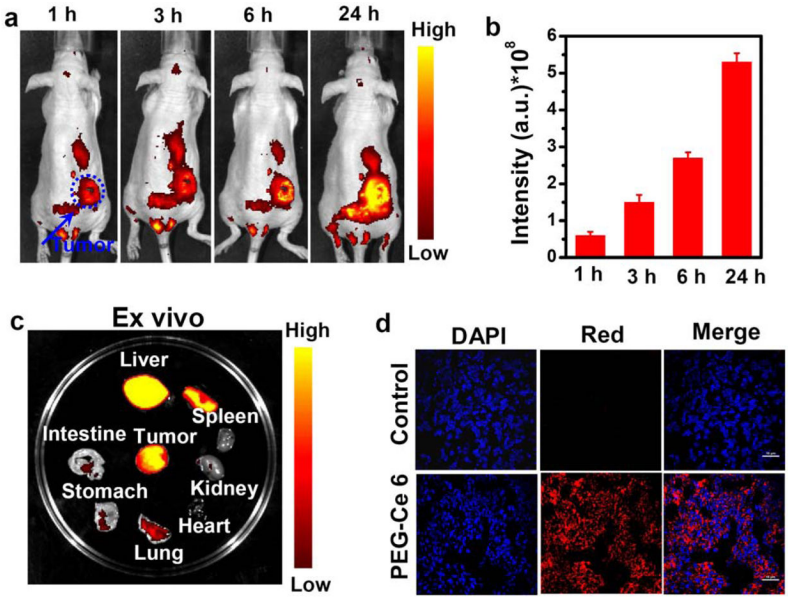

Figure 5.

In vivo and *ex vivo* fluorescence imaging. (**a**) *In vivo* fluorescence images of 4T1 tumor-bearing nude mice taken at different time points post *i.v.* injection of PEG-Ce 6 nanomicelles. Tumors are indicated by blue arrowheads. (**b**) Relative fluorescence intensities of the tumors at different time intervals based on *in vivo* fluorescence images shown in (**a**), n = 3. (**c**) *Ex vivo* fluorescence images of major organs and tumor dissected from mice injected with PEG-Ce 6 nanomicelles at 24 h p.i.. (**d**) Confocal images of tumor tissues after *i.v.* injection PEG-Ce 6 nanomicelles or not at 24 h p.i.. Red color represents the fluorescence signal from Ce 6. The scale bar is 10 μm.

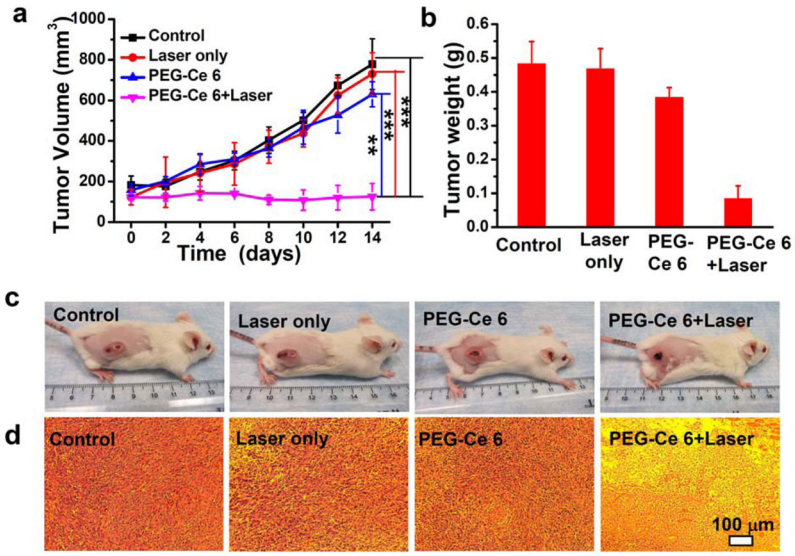

Figure 6.

In vivo PDT. (**a**) Tumor growth curves of different groups of mice after various treatments indicated. For the treatment group, four mice injected with PEG-Ce 6 at 24 h p.i. were exposed to the 658-nm laser (50 mW/cm^2, 30 min). Other three groups of mice were used as controls: untreated (Control, n =4); laser only without PEG-Ce 6 injection (Laser only, n =4); PEG-Ce 6 injected but without laser irradiation (PEG-Ce 6, n = 4. Error bars were based on SD. Statistical analysis was calculated by the methodology of Tukey's post-test (***p <0.001, **p < 0.01, or *p < 0.05). (**b**) Tumor weight of different groups taken at the 14th day. (**c**) Representative photographs of mice from different groups taken at the 14th day. (**d**) H&E stained tumor slices collected from different groups of mice on the following day after various treatments.